

---

# Eye micro-movements improve stimulus detection beyond the Nyquist limit in the peripheral retina

---

**Matthias H. Hennig and Florentin Wörgötter**

Computational Neuroscience

Psychology

University of Stirling

FK9 4LR Stirling, UK

{hennig,worgott}@cn.stir.ac.uk

## Abstract

Even under perfect fixation the human eye is under steady motion (tremor, microsaccades, slow drift). The “dynamic” theory of vision [1, 2] states that eye-movements lower hyperacuity thresholds. According to this theory, eye movements are thought to create variable spatial excitation patterns on the photoreceptor grid, which will allow for better spatiotemporal summation at later stages. We reexamine this theory with a realistic model of the vertebrate retina, comparing responses of a resting and a moving eye. The performance of simulated ganglion cells in a hyperacuity task is evaluated by ideal observer analysis. We find that in the central retina eye-micromovements have no effect on the performance. Here optical blurring limits vernier acuity. In the retinal periphery however, eye-micromovements clearly improve performance. Based on ROC analysis, our predictions are quantitatively testable in electrophysiological and psychophysical experiments.

## 1 Introduction

Normal visual acuity is limited by the photoreceptor distance on the retina to about  $1'$  of visual angle, which is determined by the neural nyquist sampling limit. The human visual system, however, is able to resolve certain stimuli (e.g. vernier stimuli) at a much higher resolution of  $< 5''$ . This effect, called hyperacuity, has given rise to a large number of psychophysical studies and several qualitative theories about perception as well as the underlying neuronal behavior in the retina. Most notably are the so-called “dynamic” and “static” theories of vision [3], which claim that hyperacuity would require eye-micromovements (microtremor, microsaccades) or not. Along the dynamic theory it has been suggested by Averill and Weymouth [1] and later by Marshall and Talbot [2] that small eye-movements would shift the photoreceptor grid across the stimulus leading to a better discriminability when appropriate spatiotemporal integration is used.

In a previous study we had designed a highly detailed model of the vertebrate retina [4]. This allows us for the first time to quantitatively test the Marshall-Talbot theory under dif-

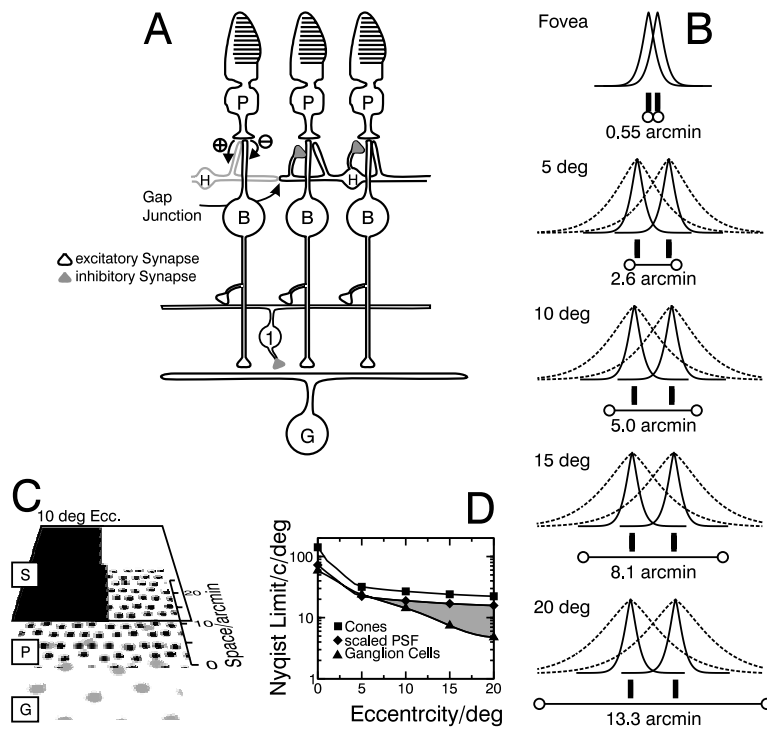


Figure 1: Overview of the model. A Structure of the retina model. Photoreceptors (P) connect to horizontal (H) and bipolar cells (B). Horizontal cells antagonize bipolar cells. Bipolar cells provide the center input to ganglion cells (G) and the surround is mediated by a Type 1 (I) amacrine cell [4]. B Scaling of optical point spread functions (top curves), photoreceptor (bars) and ganglion cell separation (lines, values are shown) at different retinal eccentricities. PSF's are shown for the constant (straight lines) and variable cases (dashed lines). C Spatial layout of the stimulus (S) and the photoreceptor (P) and ganglion cell (G) grids. D Nyquist frequencies for photoreceptors, P ganglion cells and the scaled PSF as function of the eccentricity. Aliasing occurs in the shaded region for the scaled PSF.

ferent experimental conditions. We will show that the presence of eye-micromovements indeed improves hyperacuity. Contrary to earlier assumptions we find that eye micromovements have no effect in the central part of the retina, where optical blurring defines the limit for hyperacuity tasks. At above  $10^\circ$  in the retinal periphery, however, eye-micromovements are clearly improving hyperacuity. Our approach relies on a model free (receiver-operator characteristic, ROC) analysis [5], and the reported results should be directly measurable in retinal ganglion cells and psychophysically.

## 2 MATERIALS AND METHODS

The model used in this study is based on a previously described model of the light adapted retina. In this section, we only describe the aspects which are important in the context of this study. For a detailed description and discussion of the model, see [4].

Briefly, the model consists of cone photoreceptors, horizontal and bipolar, amacrine and ganglion cells (Fig.1A). The cells are arranged on homogeneous two-dimensional noisy hexagonal grids (Fig.1C). Cones, bipolar and ganglion cells form a feed-forward path and

horizontal and amacrine cells two lateral layers. Densities and sizes of photoreceptors and ganglion cells were adjusted to the anatomical data available for the human retina (Tab.1 and Fig.1B). The density of bipolar and amacrine cells was set equal to the cone density.

Eccentricity [deg]	Cone separation [arcmin]	PC separation [arcmin]	Vernier offset [arcsec]
0	0.55	0.55	14.4
5	1.88	2.42	60
10	2.23	4.00	120
15	2.49	8.10	192
20	2.68	11.44	316

Table 1: Spatial scaling in the human retina. Cone separation was estimated from data given in [6]. Ganglion cell separation data was taken from [7]. On P cell (PC) separation was assumed equal to the dendritic tree diameter. The vernier offset is scaled proportional to the ratio of the cone to ganglion cell density.

The photoreceptor model is a slightly modified version of the mathematical description given in [4]. It is originally based on a description by [8] and the voltage responses were tested against experimental data from the macaque by [9]. To account for the sustained responses for strong, but brief stimuli, the single initial activation stage [4] was replaced by three cascaded low-pass filters. The current study focuses on human P On-center cells (or “midget” cells) from which receptive field size and density were taken according to anatomy (Tab.1). The center and surround input of both cell types is weighted by overlapping Gaussian profiles [10], where the surround extends over 6.7 times the center input [11].

Before the stimulus excites the photoreceptors, it traverses the imperfect optics of the eye. This optical blurring has been accounted for by convolving the stimulus with the point-spread function (PSF) estimated by Westheimer et al. [12] for the fovea:

$$PSF(\rho) = 0.933 \cdot e^{-2.59 \cdot \rho^{1.36}} + 0.047 \cdot e^{-2.34 \cdot \rho^{1.74}} \quad (1)$$

$\rho$  is the radius in arcmin. For higher eccentricities two sets of simulations were performed, one with a constant and one with a variable width of the PSF (Fig.1B). The first case is an approximation of the case when off-axis refractory errors of the ocular optics are corrected [13]. Then aliasing occurs at the level of the cone mosaic. In fact the optical quality of the eye varies strongly between subjects and cases have been reported where foveal vision was sampling- rather than diffraction-limited [14]. In the latter case the PSF was scaled proportional to the cone separation in order to emulate the off-axis astigmatism and increasing cone aperture. Then no aliasing occurs at the cone level, but from about  $10^\circ$  eccentricity upwards undersampling at the ganglion cell level begins due to the increasing difference between cone and ganglion cell separation (Fig.1D).

Eye micromovements were introduced by moving the retina randomly relative to the stimulus. The movements were calculated from Gaussian white noise with a mean frequency of 80Hz and a variance of 20Hz. A typical vernier stimulus has been used in the simulations. To remove the effect of the stimulus size, we used a bipartite field of 100% contrast with a small horizontal displacement in the vertical half (Fig.1C). Simulations were carried out at five different retinal eccentricities: in the fovea and at 5, 10, 15 and 20deg. The vernier offset was scaled with increasing eccentricity proportional to the ratio of the cone to ganglion cell separation (Tab.1).

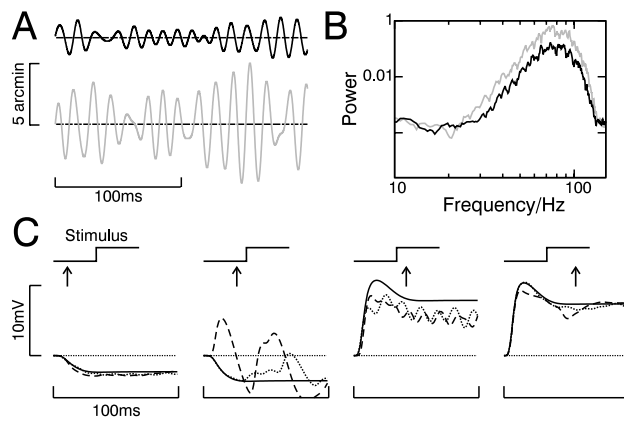


Figure 2: Characteristics of the simulated eye-micromovements. A Traces of the horizontal retinal displacement for the two tremor amplitudes used in this study (37'' and 74''). B Power spectra of the two cases from part A. C Responses of P-ganglion cells to a contrast step (100% contrast) without tremor (solid line) and with tremor (dotted line: 37'', dashed line: 74''). Horizontal alignment corresponds to the location of the cell relative to the stimulus (arrows in insets).

### 3 Results

Fig.2 summarizes the characteristics of simulated eye-micromovements. In part A an example for the horizontal displacement of the retina is shown for two tremor amplitudes. Part B shows the corresponding power spectra. Their peaks are centered at 80 Hz and frequencies range from 30 to 150 Hz. These spectra are similar to recordings from [15], but the low frequency slow drift movements have been omitted here. Fig.2C shows the membrane potential of a simulated ganglion cell at different locations relative to a contrast step with and without tremor. When the cell is located in the dark section of the contrast step, the tremor moves the light section of the stimulus into its receptive field, causing frequent strong depolarizations. For the reverse case, when the dark section of the stimulus moves into the receptive field of a cell which was previously located under the light section, the membrane potential hyperpolarizes. These hyperpolarizations are weaker than the depolarizations in the former case because the photoreceptor response is asymmetric with respect to the on- and offset of light. Light onset causes a brief strong transient response whereas offset a comparable slower response decay [4, 9].

Fig. 3A,E show the spatial response distribution on the ganglion cell layer 30ms after stimulus onset for two retinal eccentricities (5° and 10°, vernier offset 45'' and 90'', respectively) for a constant PSF width over all eccentricities. At 5° eccentricity the vernier offset is well visible by eye by comparing the upper and lower half of the responses. At 10° however, upper and lower half look very similar, implying that vernier detection is not possible.

To quantify the detectability of a vernier stimulus we performed a ROC analysis of the spatial response profiles. This procedure is shown in Fig.3: First a horizontal cross-section of the spatial response profile is taken at the ganglion cell layer for the upper and lower part of the stimulus (B,F). The detectability of a vernier stimulus should be reflected in the population average of the ganglion cell responses for upper and lower part of the stimulus. This assumption reflects the known convergence properties of the primary visual pathway, where each cortical cell receives input (via the LGN) from many ganglion cells. Thus, we

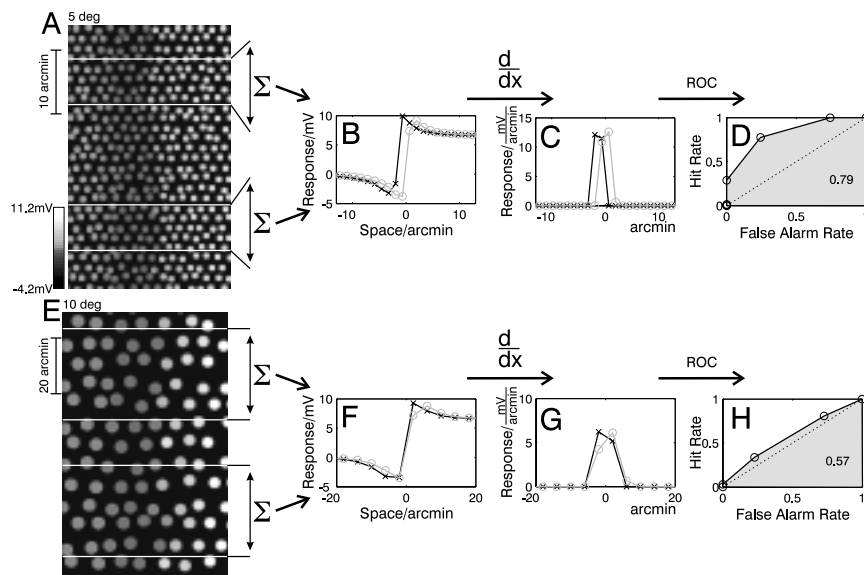


Figure 3: Spatial analysis of the vernier stimuli. A Spatial response profiles of the ganglion cells to a vernier stimulus 30ms after stimulus onset ( $5^\circ$  retinal eccentricity, vernier offset  $45''$ ). The membrane potential is coded by gray levels. B Spatial response profile for the upper (black) and lower half (grey) of the responses in A. The curves show an average over five rows. C Spatial derivative of the curves in B. The curves are rectified at zero (resting potential). D ROC curve calculated from the curves in C. Value of the integral of the ROC curve (shaded gray) is shown in the lower right part of each curve (detectability index). E-H The same analysis at  $10^\circ$  retinal eccentricity and a vernier offset of  $90''$ .

use always an average of five rows of the ganglion cell activity for analysis. The resulting profiles closely fit cumulative Difference of Gaussians functions, which is a consequence of the ganglion cell receptive field structure. In the next step, the spatial derivative of the response profile is calculated and rectified at the resting potential (C,G). This operation is similar to a cortical edge detection mechanism [16] and leads to Gaussian-like distributions. From these curves it is possible to directly compute a receiver-operator (ROC) curve (D,H). The integral of the ROC curve, ranging from 0.5 to 1, is then taken as a direct measure of the detectability of the vernier offset. This methods combines the standard, model-free ROC-type analysis with basic assumptions about the convergence properties in the primary visual pathway.

The examples in Fig.3 show the static case, without eye movements, when detectability is constant over time during the whole stimulus presentation (after 20ms of equilibration). Eye-movements lead to temporal changes of the detectability. Thus, the integral of the ROC curve, which we will call the “detectability index” (DI), will then vary over time. Fig. 4A shows this effect for five different retinal eccentricities and different tremor amplitudes using a constant PSF. For each eccentricity, the stimulus has been placed at five different locations relative to the ganglion cell receptive fields. We found, that without eye-micromovements and increasing eccentricities the detectability strongly depends on the location of the stimulus in the receptive field. This is not surprising when one considers that both the photoreceptor and ganglion cell layer undersample the image. At the fovea visual resolution is limited by the optics of the eye. At  $10^\circ$  eccentricity, there are substantial “gaps” in the cone representation of the stimulus (see Fig.1B) which cause aliasing effects. Additional undersampling occurs at the ganglion cell layer, also beginning at  $10^\circ$

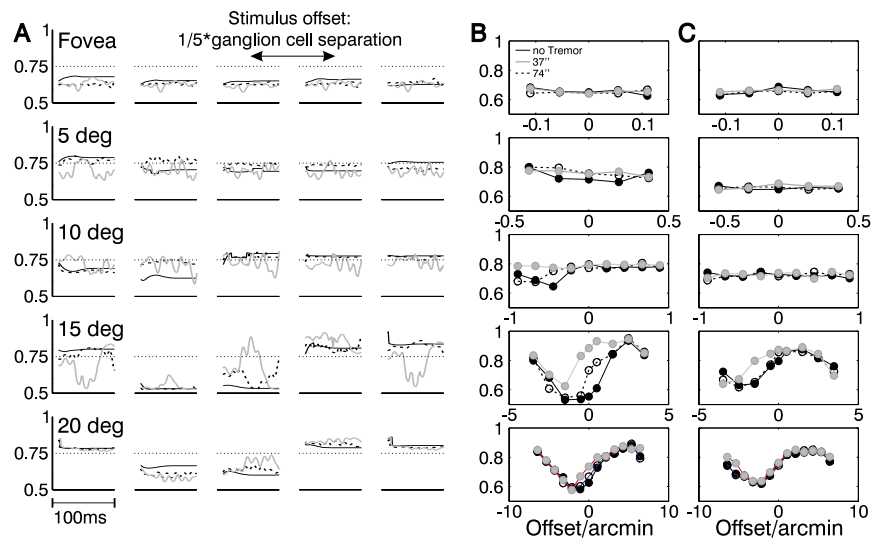


Figure 4: Temporal analysis of the ROC curves. A Detectability index as function of time at different retinal eccentricities and different stimulus displacements relative to the ganglion cell positions (black curves: resting eye, dotted curves: tremor amplitude 37'', grey curves: tremor amplitude 74''). The stimulus was shifted stepwise with an increment of a fifth of the ganglion cell separation. B Maximum of the curves in A at each eccentricity. Only these values are considered as a maximum where the DI stays above the mean for at least 10ms. C Maximal DI for the variable PSF (PSF scaled proportional to the ganglion cell separation).

retinal eccentricity. Thus undersampling at two sampling stages causes the aliasing in the detectability of the vernier stimuli. Aliasing in the periphery due to undersampling has been reported human psychophysics [17].

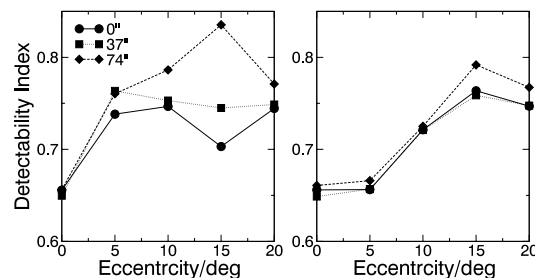


Figure 5: Mean detectability index for the experiments in Fig.3A (left, constant PSF) and B (right, PSF scaled proportional to cone-ganglion cell convergence ratio) as function of the retinal eccentricity.

Adding tremor leads to clearly visible effects in Fig.4A. The noisy curves are now randomly oscillating across the smooth curves without tremor. We note for most curves obtained with tremor there is an interval of at least 10ms where the D is above its mean and equal or above the noise-free equivalent. Psychophysical evidence shows that detection tasks require only short periods of as little as 5ms where the detectability must exceed detection threshold. Thus, eye-movements do not necessarily lead to a reduced detectability regardless of retinal

eccentricity and stimulus positioning. On the other hand we find that for eccentricities of above  $10^\circ$ , the detectability index is often substantially above the noise-free value. Thus, at increasing eccentricities from  $10^\circ$  upwards, the tremor has a beneficial effect on the detectability by reducing aliasing.

In Fig.4B, the maximum of each curve in part A is plotted as function of the stimulus position in the receptive field. Here a maximum is defined as the largest value of the detectability index within a 10ms windows. The curves show the same effects as described above: Performance remains the same in the central and improves in the peripheral retina. If the mean value of the detectability index instead of the maximum is taken, the effect is similar in the fovea, but a weaker performance increase is achieved in the periphery (not shown). Fig.4C shows the same analysis of responses for a PSF scaled proportional to the cone separation (see Fig.1B). Aliasing without tremor is weak at  $10^\circ$  as compared to Fig.4B, but significant at  $15^\circ$ . As a consequence, eye-micromovements have the same effect on performance but at larger eccentricities only.

To summarize the previous findings, the mean value of each curve in Fig.4B and C is calculated. This value can be interpreted as the psychophysical performance of a subject after many stimulus repetitions. They are shown in Fig.5A for the constant and Fig.5B for the scaled PSF. Without tremor, the detectability increases with eccentricity because of the scaling of the stimulus proportional to the cone convergence ratio to ganglion cells. The dip at  $15^\circ$  for a constant PSF results from the unproportional scaling of ganglion cell receptive field size and cone density, which both influence detectability. This effect is absent for the scaled PSF because cone undersampling is prevented. For a constant PSF, tremor increases the detectability at all eccentricities except in the fovea. The peaks for the two different tremor amplitudes are located at different eccentricities. This is a result of the scale at which undersampling occurs. The tremor with mean amplitude of  $37''$  reaches adjoining cones at  $5^\circ$  best, while  $74''$  is the range of the ganglion cell separation at  $15^\circ$ . For the scaled PSF, the effect of the weak tremor is abolished because aliasing is prevented at  $5^\circ$ , thus the PSF limits the detectability. However, the large tremor has a substantial effect at  $15^\circ$  and  $20^\circ$ .

## 4 Discussion

Our results suggest that eye-micromovements contribute to visual hyperacuity in the peripheral visual field. By simulating responses to vernier stimuli with a realistic model and applying model-free ideal observer analysis, we show that in the retinal periphery eye-micromovements reduce the effect of aliasing due to neural undersampling. This leads to a higher detectability of hyperacuity stimuli. There has been a successful attempt to use small, continuous "scanning" movements to increase the resolution of a low resolution sensor array as a technical application [18]. We show that this principle can indeed be used by vertebrates to improve visual acuity in certain (hyperacuity) tasks. However, these movements at the same time have the reverse effect on stimuli that require aliasing for detection such as high-frequency gratings [17]. Therefore it is important to note that physiological eye-micromovements do not completely remove aliasing effects. Packer and Williams [19] who show for a high frequency grating detection task contrast thresholds are low for very brief and long presentation durations. For intermediate presentation times the threshold increases substantially. Because detection relies on aliasing, it requires a resting eye. This is more likely for very brief and long presentation times. For intermediate intervals, motion prevents aliasing. Thus in our vernier detection experiment, eye-micromovements increase detectability and we expect an asymptotic decrease of thresholds as function of the presentation time.

The question arises how eye-micromovements affect human psychophysical performance. For a psychophysical experiment we predict a significant difference in the minimal stimu-

lus presentation time for an optimal performance to vernier targets between the central and peripheral retina. We would also expect an increase of detection thresholds under stabilized eye conditions in the peripheral retina. It is further possible to apply the experimental procedure that was used in this work in an electrophysiological study. Specifically, it is possible to record from one ganglion cell with many different stimulus locations. These responses can then be used to reconstruct a spatial response profile equivalent to our simulated activity distribution (Fig.3B,F). Then ROC analysis can be applied also to this data. We expect a quantitatively similar scaling of the detectability and differences between the cases with and without eye-movements.

## References

- [1] H.L. Averill and F.W. Weymouth. Visual perception and the retinal mosaic. II. The influence of eye-movements on the displacement threshold. *J Comp Psychol*, 5:147–176, 1925.
- [2] W.H. Marshall and S.A. Talbot. Recent evidence for neural mechanisms in vision leading to a general theory of sensory acuity. *Biol Symp*, 7:117–164, 1942.
- [3] R.M. Steinman and J.Z. Levinson. *Eye movements and their role in visual and cognitive processes*, chapter The role of eye movement in the detection of contrast and spatial detail, pages 115–212. Elsevier Science, 1990.
- [4] M.H. Hennig, K. Funke, and F. Wörgötter. The influence of different retinal subcircuits on the nonlinearity of ganglion cell behavior. *J Neurosci*, 22:8726–8738, 2002.
- [5] H.B. Barlow, W.R. Lewick, and M. Yoon. Responses to single quanta of light in retinal ganglion cells of the cat. *Vision Res*, 11(Suppl. 3):87–101, 1971.
- [6] J. Sjöstrand, V. Olsson, Z. Popovic, and N. Conradi. Quantitative estimations of foveal and extra-foveal retinal circuitry in humans. *Vision Res*, 39:2987–2998, 1999.
- [7] A.K. Goodchild, K.K. Ghosh, and P.R. Martin. Comparison of photoreceptor spatial density and ganglion cell morphology in the retina of human, macaque monkey, cat, and the marmoset callithrix jacchus. *J Comp Neurol*, 366:55–75, 1996.
- [8] J.L. Schnapf, B.J. Nunn, M. Meister, and D.A. Baylor. Visual transduction in cones of the monkey macaca fascicularis. *J Physiol*, 427:681–713, 1990.
- [9] D.M. Schneeweis and J.L. Schnapf. The photovoltage of macaque cone photoreceptors: adaptation, noise and kinetics. *J Neurosci*, 19(4):1203–1216, 1999.
- [10] R.W. Rodieck and J. Stone. Analysis of receptive fields of cat retinal ganglion cells. *J Neurophysiol*, 28:833–849, 1965.
- [11] L.J. Croner and E. Kaplan. Receptive fields of P and M ganglion cells across the primate retina. *Vision Res*, 35(1):7–24, 1995.
- [12] G. Westheimer. *Handbook of Perception and Human Performance*, volume 1, chapter The eye as an optical instrument. John Wiley & Sons, New York, 1986.
- [13] D.R. Williams, P. Artal, R. Navarro, M.J. McMahon, and D.H. Brainard. Off-axis optical quality and retinal sampling in the human eye. *Vision Res*, 36:1103–1114, 1996.
- [14] D.T. Miller, D.R. Williams, G.M. Morris, and J. Liang. Images of cone photoreceptors in the living human eye. *Vision Res*, 36:1067–1079, 1996.
- [15] A. Spauschus, J. Marsden, D.M. Halliday, J.R. Rosenberg, and P. Brown. The origin of ocular microtremor in man. *Experimental Brain Research*, 126, 1999.
- [16] D.H. Hubel and T.N. Wiesel. Receptive fields, binocular interaction, and functional architecture in the cat’s visual cortex. *J Physiol*, 160:106–154, 1962.
- [17] L.N. Thibos, D.J. Walsh, and Cheney F.E. Vision beyond the resolution limit: aliasing in the periphery. *Vision Res*, 27:2193–2197, 1987.
- [18] Landolt O. and Mitros A. Visual sensor with resolution enhancement by mechanical vibrations. *Autonomous Robots*, 11:233–239, 2001.
- [19] O. Packer and D.R. Williams. Blurring by fixational eye movements. *Vision Res*, 32:1931–1939, 1992.